Flow structure and seasonality in the Hebridean slope current

Alejandro J. SOUZA*#, John H. SIMPSON, M. HARIKRISHNAN, Jonathon MALARKEY

School of Ocean Sciences, University of Wales Bangor, Menai Bridge, Anglesey LL59 5EY, UK

Abstract – The intensity, structure and variability of the slope current have been determined from 16 months of observations with Acoustic Doppler Current Profilers (ADCP) and conventional current meters on a cross-slope section at the Hebridean shelf edge during the Shelf Edge Study (SES) programme. After removal of the tidal signals, the mean flow over the upper slope is found to be closely parallel to the topography with speeds of ≈ 20 cm·s^{-1}. The flow extends down to a depth of 500 m and is predominantly barotropic, especially in winter when the flow is practically uniform between 350 m and the surface. In summer, there is a significant baroclinic component with a pronounced maximum in current at a depth of about 200 m but more than 80% of the kinetic energy is in the barotropic component. Flow in the core of the current is highly persistent with the Neumann's steadiness St > 0.8 in summer. In winter the flow is generally more energetic and variable and extends onto the adjacent shelf. The cross-slope profile of sea surface elevation, computed from the mean barotropic currents, shows a consistent relation to seabed topography through the seasonal cycle. Long-term averages of the cross-slope components are generally small (≈ 2 cm·s^{-1}) with some indication of persistent down-slope flow in the bottom Ekman layer. Measurements with shipboard ADCP on sections at intervals along the slope show a high degree of continuity in the structure of the flow. The core of the flow appears to be related to a weak positive salinity anomaly and a depression of the 9.5 °C isotherm near the shelf, but there is no strong correlation between the core of the slope-current and the core of the salinity anomaly. It is proposed that this may be due to differences in the cross-stream diffusion of salt and momentum which have different boundary conditions at the slope. The observed cross-stream structure of the current supports the hypothesis that JEBAR is the principal forcing mechanism but the result cannot be regarded as conclusive since a uniform potential vorticity model of the flow produces a similar cross-sectional structure of the current. © 2001 Ifremer/CNRS/IRD/Éditions scientifiques et médicales Elsevier SAS

Résumé – Structure et variations saisonnières du flux dans le courant de talus continental du plateau des Hébrides. L'intensité, la structure et la variabilité du courant de talus continental ont été déterminés par des mesures effectuées pendant seize mois à l'aide et de courantomètres à effet Doppler (ADCP) et conventionnels au large des îles Hébrides pendant le programme *Shelf Edge Study* (SES). Après élimination du signal des marées, le flux moyen sur la partie supérieure du talus suit la topographie avec des vitesses d'environ 20 cm·s^{-1}. Jusqu'à une profondeur de 500 m le flux est principalement barotrope, en particulier l'hiver où il est pratiquement uniforme entre la surface et 350 m. En été, une composante barocline est discernable avec un courant maximal prononcé vers 200 m de profondeur, mais plus de 80% de l'énergie cinétique est barotrope. Le flux au centre du courant est très constant avec un indice de stabilité de Neumann St supérieur à 0,8 en été. En hiver le flux, généralement plus fort et variable, s'étend sur le plateau continental. L'élévation de la surface des eaux calculée à partir des courants barotropes moyens suit la topographie des fonds tout au

*Correspondence and reprints.
E-mail address: ajso@pol.ac.uk (A.J. SOUZA).
#Present address: Centre for Coastal & Marine Sciences, Proudman Oceanographic Laboratory, Bidston Observatory, Bidston Hill, Prenton CH43 7RA, UK

long du cycle saisonnier. Les moyennes à long terme des composantes du courant transversal au talus sont généralement faibles (≈ 2 cm·s^{-1}) et rèvèlent un flux descendant persistant au bas de la couche d'Ekman. La courantométrie sur des sections transversales au talus continental indique que la structure du flux est fortement continue. La veine centrale du courant semble associée à une légère anomalie positive de la salinité et à une dépression de l'isotherme de 9,5 °C près du plateau continental, mais sans corrélation marquée entre les positions du courant et de l'anomalie en sels. Cela pourrait être du aux différences entre le moment et la diffusion des sels à travers les courants, tous deux présentant des conditions aux limites distinctes sur la talus continental. La structure transversale du courant confirme l'hypothèse selon laquelle JEBAR est le principal mécanisme de forçage, mais ce résultat n'est pas concluant étant donné qu'une modélisation du flux avec une vorticité potentielle uniforme produit une structure similaire. © 2001 Ifremer/CNRS/IRD/Éditions scientifiques et médicales Elsevier SAS

slope current / seasonality / velocity structure

courant de talus / variation saisonnière / structure du flux

1. INTRODUCTION

Although on long time scales the ocean is a single mixed system, as the consistency of its chemical composition testifies, its dynamics is generally discussed in terms of separate deep-ocean and shelf sea systems. The processes operating in each of these contrasting regimes are increasingly well understood. Much of the deep ocean is permanently stratified with weak, predominantly geostrophic currents. Wind stirring acts at the surface to mix a relatively thin surface boundary layer. Tidal motions are generally weak, and in combination with the mean flow, form a bottom boundary layer of limited height. Most of the volume is in the rather tranquil, stratified interior region where geostrophy rules and energy dissipation is low. By contrast, the shelf is a high-energy system and constitutes the major sink for energy inputs to the ocean, notably for the tides, but also for wave energy and other wind driven motions. The surface and bottom boundary layers have scales which are comparable to the depth so the boundary layers may overlap and frequently do.

The interface between these two contrasting systems is the shelf edge where there is usually a marked increase in seabed steepness at the top of the continental slope, starting at a depth of around 200 m. It is in this narrow region of steep topography that the distinct deep-ocean and shelf regimes adjust to each other. The processes involved in this adjustment are much less well understood than those operating in the contrasting shelf and deep-ocean systems but they are of considerable importance in that they control the exchange of water properties and particles across this key ocean boundary. Our ability to estimate, for example, important fluxes such as those of carbon and nutrients between shelf and deep ocean is extremely limited because of the lack of knowledge of the intensity, scale, and variability of cross slope motions.

Generally, we know from theory that the steep topography of the slope, together with the influence of Earth's rotation, steers the barotropic flow closely parallel to the bathymetry and thus inhibits exchange between the shelf and the ocean. In the case of steady, homogeneous flow in geostrophic balance, the sea surface elevation is directly related to the seabed topography and the largest barotropic currents, corresponding to the strongest surface gradients, should occur over the steepest part of the slope. In such pure geostrophic flow, there is no cross-isobaric motion, so all exchange depends on components of the flow, which are not subject to this geostrophic constraint.

The slope-parallel flow (the slope current) has been recognised for some time as an important feature of the slope region. While the topographic steering mechanism favours the location of strong flows over the slope it does not account for the momentum input to the slope current. Forcing of the flow is postulated to result from the combined effect of the steep topography and the meridional density gradient, the JEBAR effect (Sarkisyan and Ivanov, 1971), which generates a difference in meridional pressure gradients between ocean and shelf equivalent to a surface slope of $\approx 10^{-7}$. This gradient is sufficient to maintain a flow of the observed magnitude against frictional resistance (Huthnance, 1984; Pingree and Le Cann, 1989).

The steep topography of the shelf edge also requires radical changes in the tidal regime as the deep-ocean tide moves onto the shelf. The reduction in depth, by bringing about a reduction in the group velocity, induces an increase in the amplitude of the barotropic tidal as it crosses the slope. Moreover, under stratified conditions, a fraction of the energy flux moving onto the shelf is transferred to internal motions, which are produced as the stratified structure of the water column is moved up and down the slope. The resulting internal tide may significantly complicate the flow field at the shelf edge and is thought to enhance vertical mixing in slope regions of high tidal energy like the Celtic Sea (Pingree et al., 1983), leading to increased nutrient supply for production in the photic zone. At the Hebridean shelf edge, which is the focus of the present study, tidal energy levels are generally lower than in the Celtic Sea. However, the current speeds associated with the tidal flow are of the same order as the mean flow and need to be carefully extracted from the current field to allow determination of the residual current.

Efforts to study the slope current, and the equally significant cross-slope exchange have assumed increasing importance in relation to questions about how the shelf and deep-ocean systems interact in various aspects of biogeochemical cycling. The measurements reported here build on the previously reported study by Huthnance (1986) and extend our knowledge of the structure and seasonality of the current system. The observations were undertaken as part of the Shelf Edge Study (SES), an integrated inter-disciplinary study to establish the basis for the estimation of fluxes between the north-west European shelf and the Atlantic Ocean across the Hebridean shelf edge as part of the United Kingdom Land Ocean Interaction Study (LOIS) programme.

2. THE SES SITE AND OBSERVATIONAL PROGRAMME

The site for the observations was chosen in an area of the Hebridean shelf break (*figure 1*) which has rather regular
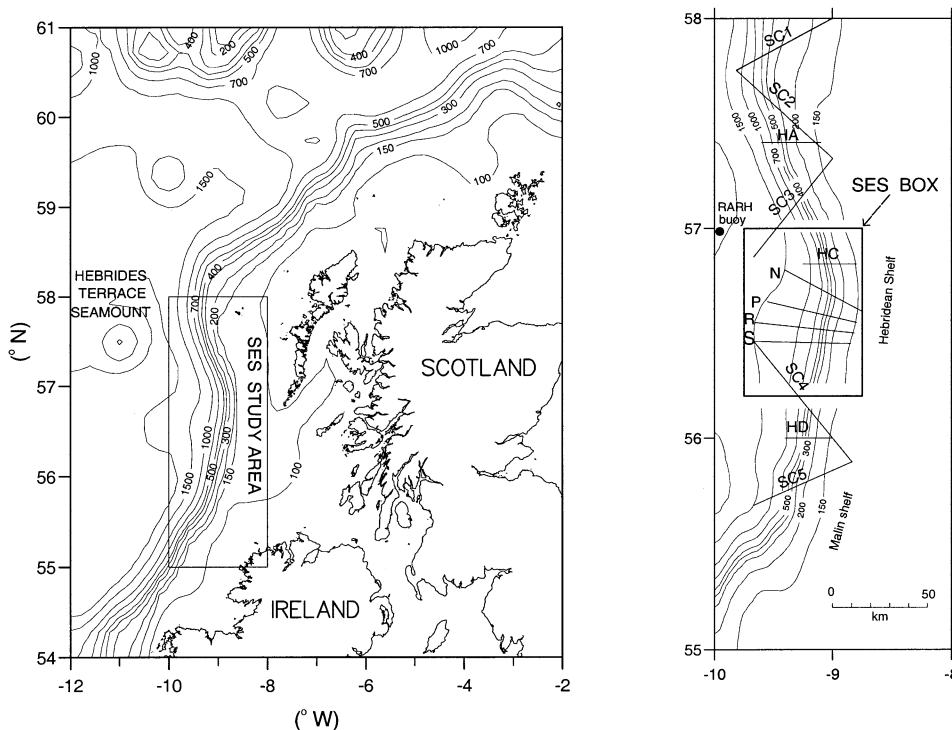

Figure 1. SES study area. (a) Location, (b) close up of the SES study area including the SES box and survey lines referred to in the text.

topography with the depth contours running almost parallel to the meridians and the depth increasing from 150 to 1 000 m in a distance of about 30 km. A more detailed picture of the topography, based on an extensive swath bathymetry survey (McCartney and Huthnance, 1995), shows the steepest gradients of order 1:10 occurring between 200 and 500 m. Further to the west, the topography is complicated by the presence of the Hebrides Terrace Seamount but this feature does not extend above 1 000 m and has little influence on the slope regime at shallower depths than this.

The winds in this region are predominantly from the southwest with mean speeds of ≈ 8 m·s^{-1}, and exhibit large variability as Atlantic depressions track in from the west. The tides are relatively small with an M_2 amplitude of ≈ 1 m and corresponding tidal streams of magnitude 15 cm·s^{-1} on the shelf diminishing to ≈ 5 cm·s^{-1} in deep water.

The core of the SES programme consisted of regular observations over a 15-month period in the SES box (*figure 1b*) bounded by the north (N) and south (S) primary lines with secondary lines between them. The principal mooring array across the shelf break was located on the S line with moorings at depths 140, 200, 300, and 700 m. Each mooring was equipped with a number of current meters, thermistor chains and transmissometers and, in the case of the shallower moorings, bottom-mounted ADCPs. The nominal distribution of the instrument is shown in *figure 2*. The time series observations were set in a spatial context by complementary hydrographic observations at intervals of approximately two months when the box and adjacent slope regions were surveyed in as much detail as weather conditions allowed.

The original aim was to maintain the S-line array for 15 months, but moorings were frequently disrupted by fishing vessels trawling along the slope parallel to the bottom contours in the depth range where our moorings were located. At times of most intense fishing (e.g. in May during the blue whiting season), it was impossible to maintain a coherent array and considerable lacunas in the data were unavoidable. Nevertheless the resulting data sets from these moorings and the complementary measurements with ARGOS drifters have added enormously to the available database on conditions at the shelf edge.

This paper presents the first results from the analysis of the new data sets concentrating on the cross-slope struc-
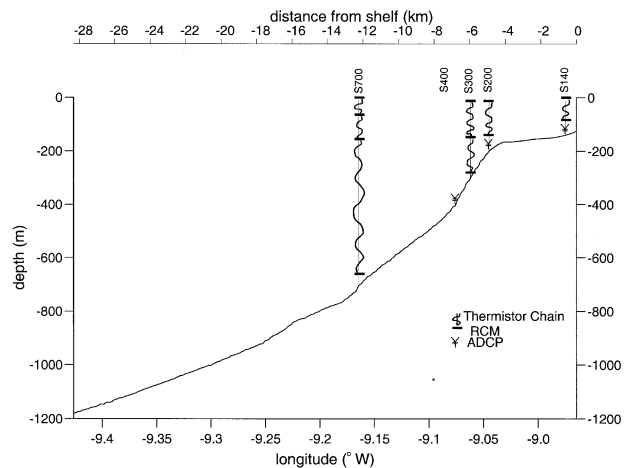

Figure 2. Mooring instrumentation schematic, showing the nominal position of instruments for line S. RCM: current meter.

ture and variability of the current field and the continuity of the slope current system along the Malin and the Hebridean shelf west of Scotland.

3. T–S STRUCTURE AND MEAN FLOW IN SUMMER AND WINTER

We have selected contrasting periods of comparable length in summer (25 days) and winter (18 days) for analysis when data coverage was most favourable. During the summer period (12 August–6 September 1995), data were obtained at five locations across the shelf, two using conventional current meter moorings (S700, S300), two using ADCP (S200 and S400) and the fifth equipped with both (S140). For the winter period (5 February–22 February 1996), the coverage was limited to three positions, one conventional current meter mooring (S700), one ADCP station (S400), and a shelf station with both ADCP and conventional current meters (S140). The results of the analysis of the separate data sets have been combined in the form of contoured plots for the shelf and slope generated by UNIRAS using linear interpolation on a grid with scales of 20 m in the vertical and 1–2 km in the horizontal.

Temperature and salinity structures representative of these periods are shown in *figure 3*. The winter period is characterised by a weak vertical structure with almost uniform conditions down to 500 m (*figure 3a*). The
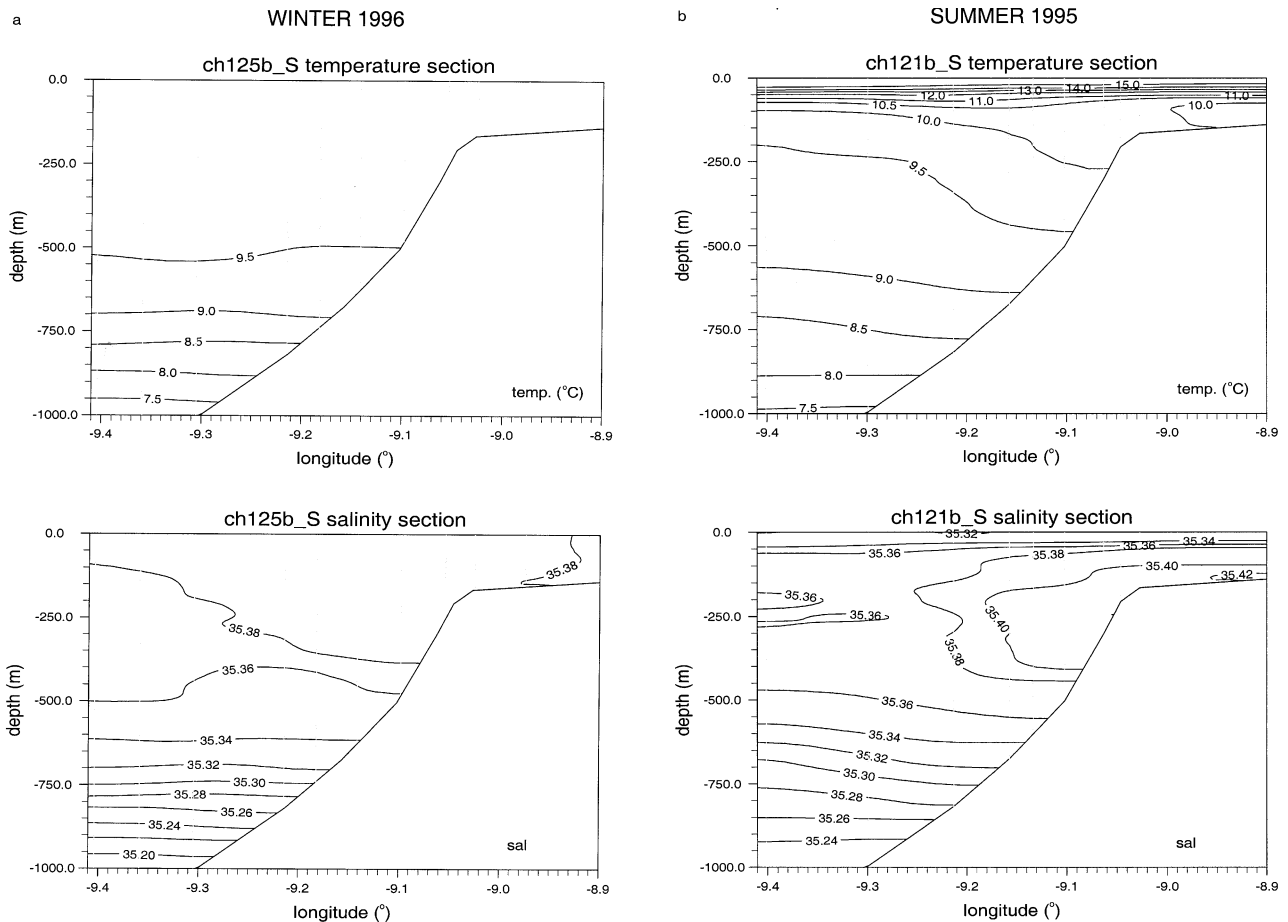
Figure 3. Temperature and salinity structure on the S line across the shelf edge. (a) Winter regime (5–22 February 1996); (b) summer regime (17 August–4 September 1995), dots show the position of the CTD measurements.

near-surface salinity exceeds the 1 000-m value by 0.16 while the corresponding temperature difference is +2 °C so that the density structure is near to neutral stability with $\Delta\sigma_\theta = 0.24 \, kg \cdot m^{-3}$.

By contrast the summer regime (*figure 3b*) involves strong stratification with the surface temperature reaching 15 °C while below 500 m, temperatures remain close to winter values. There is now a pronounced downward dipping of the isotherms (especially 9.5 °C) near the slope so that water on the slope is up to 0.5 °C warmer than at the same depth away from the slope. At the same time, the salinity distribution shows a weak subsurface maximum centred around 250 m. This warm salty water is a feature which has been postulated to result from the importing of higher salinity water from the south by the slope current (Hill and Mitchelson-Jacob, 1993). We shall return to the questions of the continuity and seasonality of the temperature–salinity structure but for the moment we focus on the flow measurements.

The ADCP and current meter data for the summer and winter periods were subjected to tidal analysis by fitting six harmonics (M_2, S_2, N_2, O_1, K_1, and M_4) to the current components using least squares techniques (Godin, 1972).

The oscillatory tidal currents were then subtracted from the original time series, to estimate the residual flows, which are presented in *figures 4* and *5*. Original data acquisition points are indicated by dots (ADCP bins) and stars (individual current meters).
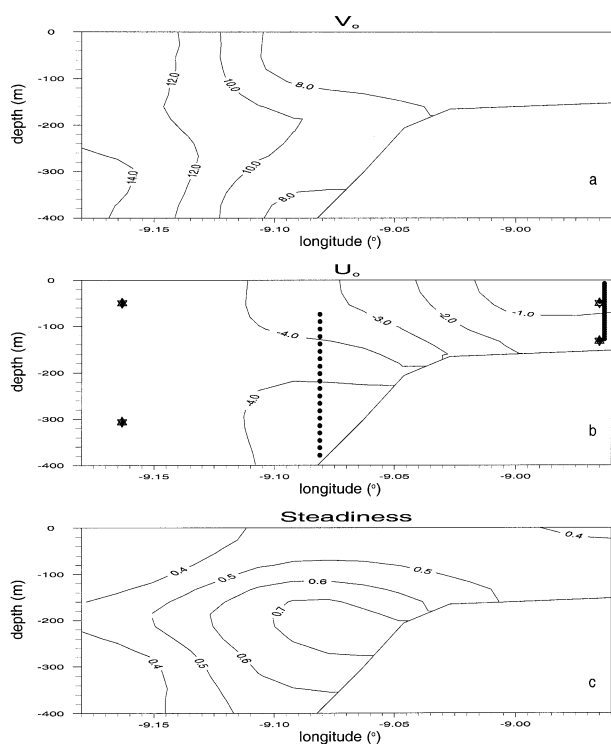
Figure 4. Mean flow and steadiness in winter regime. (a) Along-slope velocity; (b) across-slope velocity; (c) steadiness, original data location indicated by dots (ADCP bins) and stars (individual current meters).

Figure 5. Mean flow and steadiness in summer regime. (a) Along-slope velocity; (b) across-slope velocity, (c) steadiness, original data location indicated by dots (ADCP bins) and stars (individual current meters).

Both winter and summer pictures indicate sustained, along-slope poleward flow in the order of $10~\mathrm{cm \cdot s^{-1}}$ extending from the top of the slope into deep water. Whereas the winter flow (*figure 4*) is almost purely barotropic, the summer flow (*figure 5*) exhibits a mid-water maximum of $15~\mathrm{cm \cdot s^{-1}}$ at a depth of 200 m with the speed decreasing to $5~\mathrm{cm \cdot s^{-1}}$ at the surface. On the shelf, the summer mean flow diminishes rapidly to the east of S200 and is weakly southward at S140. In the winter situation mean flow $> 6~\mathrm{cm \cdot s^{-1}}$ extends onto the shelf.

Cross-slope flow (*figures 4b, 5b*) was generally weak ($2~\mathrm{cm \cdot s^{-1}}$ or less) over the whole section so that the net flow was closely parallel to the bathymetry. In winter the net cross-shelf transport over the 18-day observation period was apparently $\approx 3~\mathrm{m^2 \cdot s^{-1}}$ off the shelf at the top of the slope. In the summer period, the corresponding figure is close to zero but interestingly, there is some indication of down-slope transport down the slope at S200 and S400 where observations extend into the bottom boundary layer.
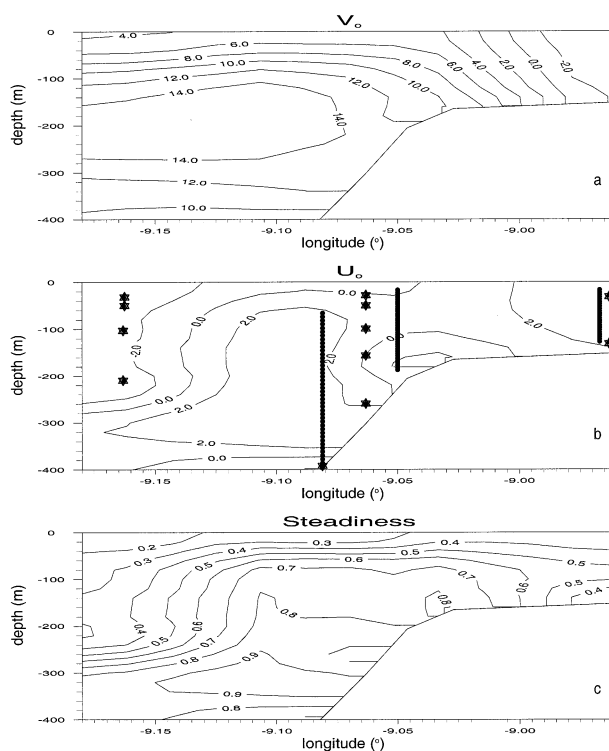
Over the slope, both in summer and winter, the flow is persistent as can be seen in *figures 4c* and *5c* which show the Steadiness factor (Neumann, 1968) defined as:

$$St = \frac{vector\,mean~U}{scalar\,mean~U} = \frac{|\overline{U}|}{\overline{|U|}} \qquad (1)$$

where $U = (u,v)$ is the velocity vector. A completely steady flow corresponds to $St = 1$. Values of St are highest over the slope, where, in summer, values exceed 0.8 for a large area of the section just below the core and reach a peak of 0.9 around 300 m depth. Lower values in winter (≈ 0.7) indicate a higher variability probably in response to increased wind forcing. In summer, the ratio of R.M.S. along-slope velocity to the mean in the core of the current is lower than 0.5 so that the flow will rarely reverse. On the shelf, the steadiness is generally much lower than over the slope and diminishes as we move away from the shelf edge to values of ≈ 0.4 at S140 in both summer and winter regimes.
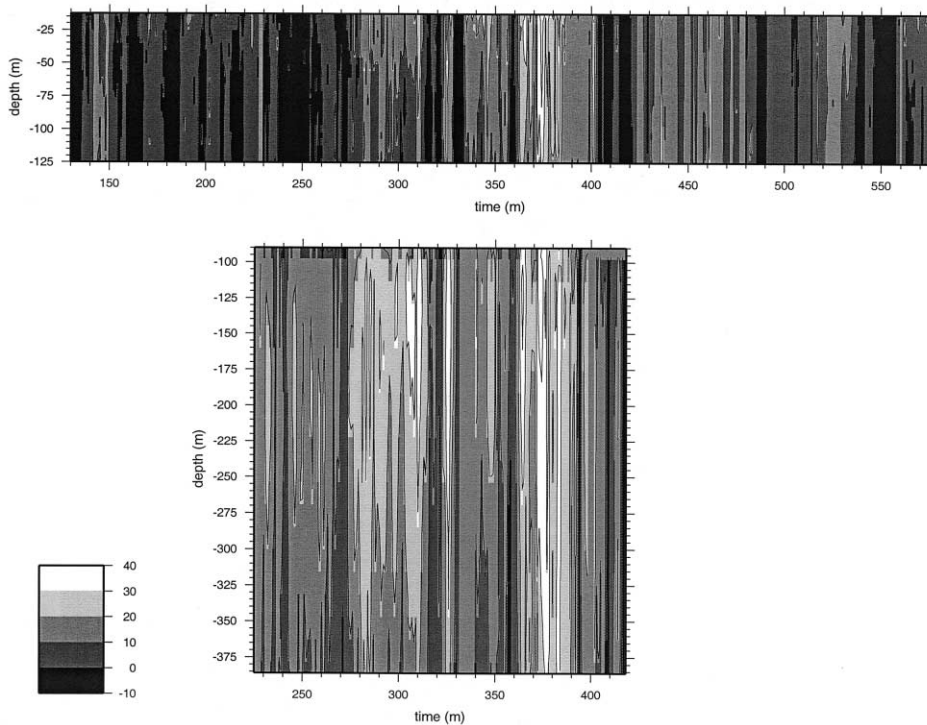
Figure 6. Time series of along-slope current from bottom mounted ADCP. (a) S140; (b) S400.

A longer time perspective of the mean slope current (*figure 6a*) confirms the persistence of the flow over a period of 190 days at S400. At this central position the flow is almost always northwards at speeds rarely below 10 cm·s^{-1} and predominantly barotropic. Peak flows of > 30 cm·s^{-1} occur at times, notably in January (day 365–385) when strong northward flows also are apparent on the shelf at S140 (*figure 6b*) along with reversals of the flow exceeding speeds of 10 cm·s^{-1}. During summer (days 140–280), the shelf flow is generally weak as in *figure 5* and variable in direction.

4. CONTINUITY OF THE SLOPE CURRENT AND T–S STRUCTURE

In an extended survey during 23–27 August 95, we explored the spatial variation in the temperature and salinity structure and flow field by making a series of cross slope CTD/XBT transects along an extensive section of the slope between 55.5° to 58°N (≈ 275 km). The results (*figure 7*) indicate a high degree of consistency in cross-slope structure of both temperature and salinity

with basic patterns similar to those of *figure 3*. On each section there is a region of relatively warm salty water apparent near, or at the top of, the slope. With increasing distance to the north, the maximum salinity of the mid-water core diminishes slightly and the volume of water on the section with S > 34.42 generally decreases. On the assumption that the T–S anomaly is associated with the slope current flowing northward, the weakening of the salinity core would signify the influence of lateral diffusion. Although present on all sections, the salinity maximum is also rather variable in position suggesting lateral excursions of the current.

In order to map the equivalent mean flow structure, it is necessary to sample repeatedly on the same section so that the tidal motions can be removed. This was achieved during a second survey in the period of 26 July to 8 August 1996 when we made measurements on three cross-slope sections 55 km apart (*figure 8*). Each section was first surveyed with closely-spaced CTD profiles from the shelf out to 1 000 m depth. Thereafter the ship steamed repeatedly backward and forward over the section for a total of 13 hours at 9 knots, which meant that
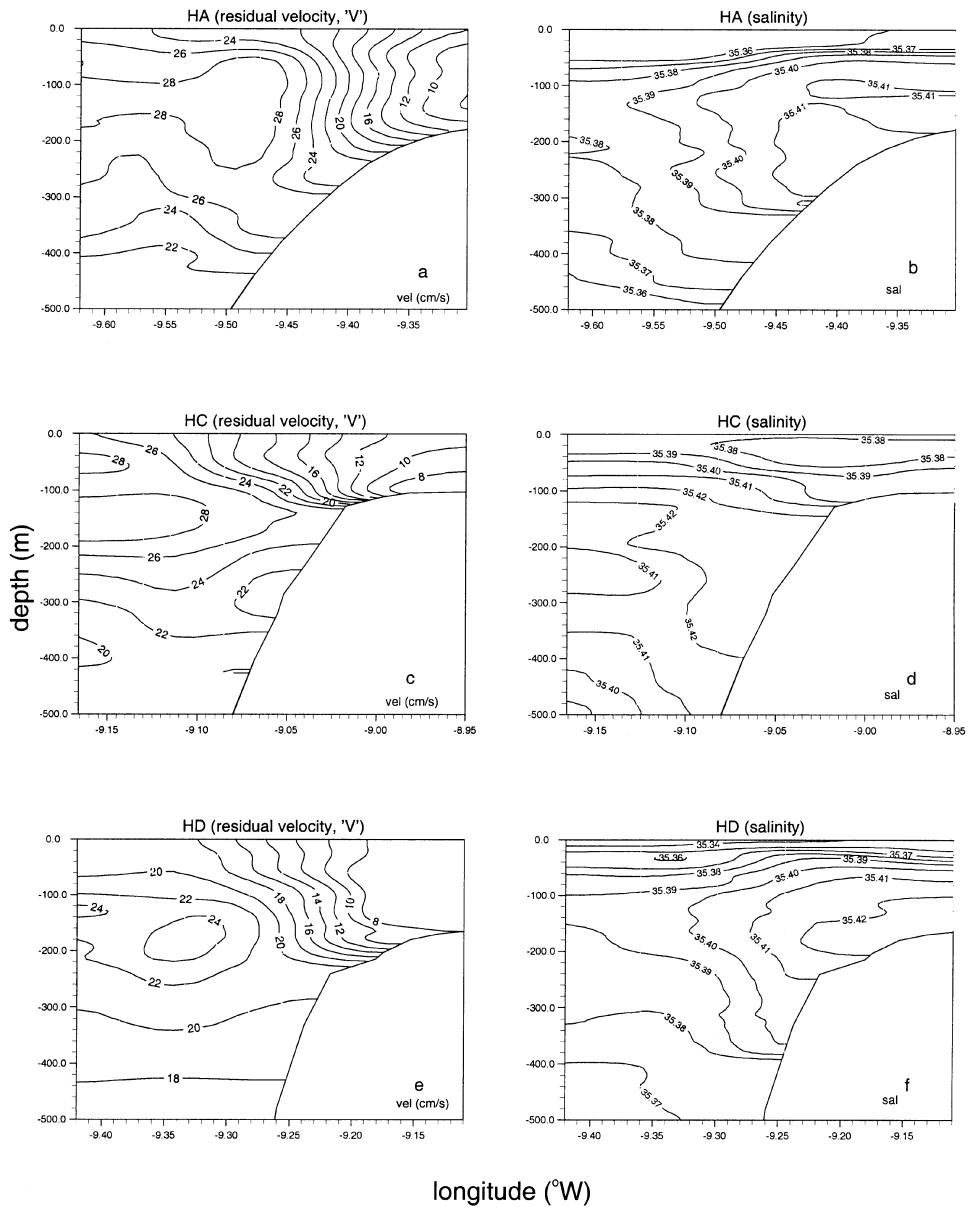
Figure 7. Along-slope temperature and salinity sections for summer 1995 continuity experiment. (a) Temperature; (b) salinity; (c) locations (doted line indicate the position of the CTD and XBT measurements).

Figure 8. Along-slope residual velocities from ADCP and salinity sections along the slope for summer 1996. (a), (c), and (e) are the residual velocities for sections HA, HC and HD respectively, while (b), (d) and (f) are the salinities for the same sections.

each station would be revisited at least six times in a tidal cycle. This procedure effectively samples the vertical flow structure at each location at intervals of approximately two hours, which allows the removal the main semi-diurnal tidal component (Simpson et al., 1990). Bottom tracking was maintained out to depths in the

order of 500 m after which we have used differential GPS navigation to recover the velocities relative to the seabed.

Examples of the resulting mean flow and the corresponding salinity are shown in *figure 8*. The water column T–S structure is closely similar to that observed in August 1995,

with a marked mid-water salinity maximum of ≈ 35.42 close to the top of the slope. The structure of the mean along-slope flow is similar on all sections with a subsurface maximum (20–28 cm·s^{-1}) located at 100–200 m depth over the slope and the speed decreasing rapidly at the top of the slope and onto the shelf. As in the mooring results for the summer regime, surface velocities over the slope are significantly reduced relative to the 100-m level, but the current is predominantly barotropic with about 80% of the energy in the depth mean component.

It is apparent from *figure 8* that the along-slope velocity field is not directly correlated with the salinity distribution; the salinity maximum is confined close to the shelf while the region of maximum flow does not reach the seabed over the slope and extends much further towards deep water. This lack of close coupling of the flow and salinity fields, which is perhaps surprising in view of the general association of the T–S anomalies with the slope current noted by Hill and Mitchelson-Jacob (1993), will be discussed further but first we consider possible dynamic inferences from the observed flow structure.

5. DYNAMICAL BALANCE IN THE FLOW

Away from the surface and bottom boundary layers, we may expect the flow in the interior region of the slope current to be close to geostrophic balance. In winter the flow is essentially barotropic; even in the summer period the barotropic component predominates with $\approx 82\%$ of the kinetic energy in the barotropic component.

In steady, barotropic, geostrophic flow, continuity requires that the Jacobian of the surface elevation η and water depth h is zero (Proudman, 1953), i.e.:

$$\frac{\partial(\eta,h)}{\partial(x,y)} = \frac{\partial\eta}{\partial x}\frac{\partial h}{\partial y} - \frac{\partial\eta}{\partial y}\frac{\partial h}{\partial x} = 0 \qquad (2)$$

which implies that the surface elevation η is a function of the water depth h only and the flow will be related to grad h and parallel to isobaths. There is no a priori basis for anticipating the form of $\eta(h)$, but on the assumption that flow is barotropic, we may derive an estimate of η from the observations using the geostrophic balance:

$$fV = g\frac{\partial\eta}{\partial x} \qquad (3)$$

where V is the depth-mean flow and f is the Coriolis parameter. *Figure 9a* shows the surface elevation ob-
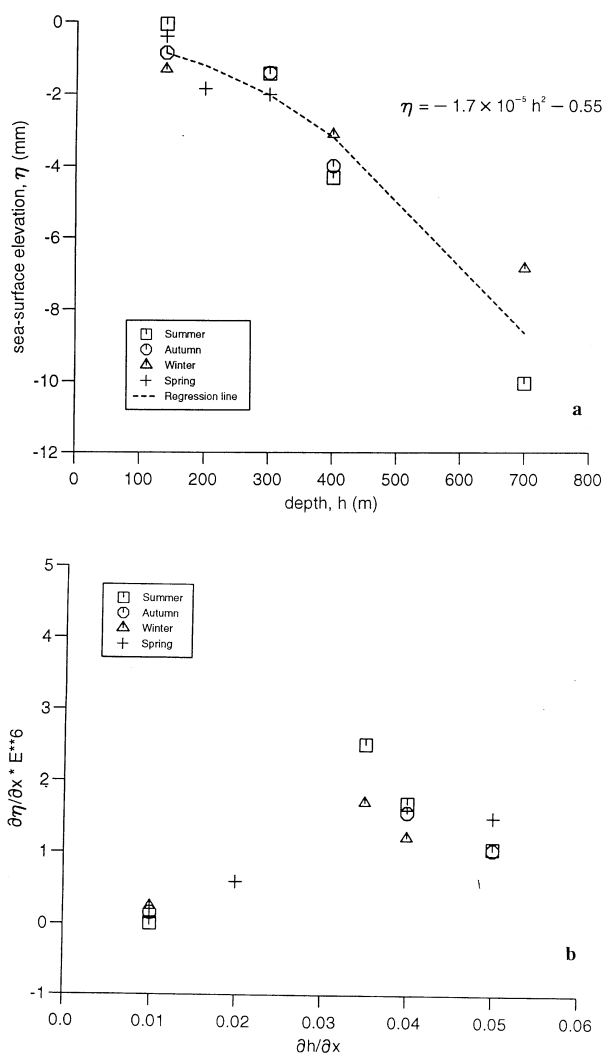

Figure 9. Sea surface topography on S line derived from barotropic geostrophic approximation. a) Elevation versus depth; b) surface gradient (barotropic geostrophic velocity) versus bottom slope.

tained by integrating the surface slope from each of the principal mooring positions across the slope. The decrease in level moving between S140 and S700 ≈ 1 cm and the functional form is apparently consistent for data from the four seasons shown and fits reasonably well to:

$$\eta(h) = -1.7x\,10^{-5}\,h^2 - 0.55 \qquad (4)$$

There are also indications that the surface and bottom slopes (*figure 9b*) are likewise consistently related in different seasons although the surface gradient does not apparently increase monotonically with bottom slope.

Although equation (2) indicates that a functional relationship between η and h exists for a steady, barotropic geostrophic flow, it does not determine the nature of the function involved. The observed structure of the current may, however, have a diagnostic value in relation to the possible driving mechanism. As mentioned in the introduction, a candidate mechanism for forcing the slope current is JEBAR (Sarkisyan and Ivanov, 1971), which involves a difference in meridional pressure gradients between ocean and shelf. In the absence of motion, the surface slope required to balance a meridional density gradient and achieve a zero depth-averaged pressure gradient ignoring friction is given by:

$$\frac{\partial \eta}{\partial y} = -\frac{1}{2}\frac{h}{\rho}\frac{\partial \rho}{\partial y} \qquad (5)$$

i.e. the sea surface slope is proportional to the water depth, for a given $\partial \rho / \partial y$. Since the density gradient does not vary greatly across the slope, the alongshore sea level decline is greatest in deep water. If the ocean and shelf sea levels are assumed to match at some upstream location, then the sea level difference between the shelf and ocean becomes progressively greater in the poleward direction, causing an increase in the strength of the poleward flowing slope current. The strengthening of the poleward flow implies along-slope convergence and hence cross-slope transport. But this contradicts the conservation of potential vorticity arguments. Also, the slope current speed would eventually become unrealistically large as the shelf–ocean sea level difference increases indefinitely in the poleward direction. Both of these problems can be resolved if the effect of bottom friction is included.

Huthnance (1984) examines the interaction between along-isobath density gradients and bathymetry governing the flows along a narrow slope. He derived a vorticity equation by cross-differentiating depth average linearised horizontal momentum equations and applying equilibrium conditions to derive a depth average current over the continental shelf and slope. The resulting along-slope component of velocity (the slope current) results from the balance of the longitudinal gradients, the bottom topography and friction:

$$V(x) = \frac{g}{2k\rho}\frac{\partial \rho}{\partial y} h(x)(H - h(x)) \qquad (6)$$

where V is the along-slope component of velocity, H is the abyssal depth where the JEBAR tends to zero, k is the linear friction coefficient and $h(x)$ is the local depth. So
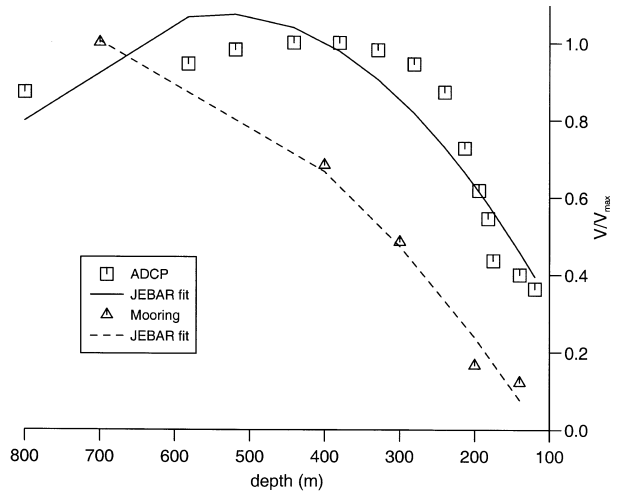

Figure 10. The JEBAR functional fit, as specified in equation (11) to depth-averaged velocity data, where the velocity has been normalised by the sectional maxima. Original ADCP data for section HA are indicated by squares and solid line represents the fit; while the mean normalised velocities from the mooring deployments are indicated by triangles and their fit by the dashed line.

we would expect a current driven by JEBAR to have a cross-slope structure conforming to $V \propto h\,(H{-}h)$. In order to test this notion, we have fitted equation (6) to our observations using least squares. *Figure 10* shows the results for both the ship-borne ADCP data from line HA and for the mean currents observed by the moorings on the S line, after the velocity has been normalised by their sectional maximum. There is a reasonable fit in both cases with H determined as 1 100 m (for the ship-borne ADCP) and 1 600 m (for the moored instrumentation). The gradient terms $h/\rho\;\partial \rho/\partial y$ was found to be of the order of 10^{-7} in agreement with results from Huthnance (1984) and Pingree and Le Cann (1989).

While the results of *figure 10* suggest that JEBAR is responsible for the forcing of the slope current, other explanations of the observed structure may be possible. We shall now briefly consider an alternative model in which it is assumed that the potential vorticity is uniform across the stream. Since the slope flow is mostly in the y direction ($v \gg u$), we assume that the relative vorticity is essentially given by $\partial V / \partial x$. Assuming that $x = 0$ is located at the velocity maximum where $\partial V / \partial x = 0$ and the depth is h_0, the uniformity of potential vorticity may be expressed as:

$$\frac{f + \frac{\partial V}{\partial x}(x)}{h(x)} = \frac{f}{h_0} \qquad (7)$$

Integrating across the stream gives the velocity:

$$V(x_1) = V_0 + \frac{f}{h_0} \int_0^{x1} (h - h_0) \, dx \qquad (8)$$

where V_0 is the maximum velocity occurring at $x = 0$. Using the geostrophic relation (3) and integrating again we have for the elevation:

$$\eta(x) = \frac{f}{g} V_0 x + \frac{f^2}{gh_0} \int_0^x \int_0^{x1} (h - h_0) dx \, dx_1 \qquad (9)$$

We have evaluated these integrals for the cross-slope topography of the S line using values of $V_0 = 0.2$ m·s^{-1} and $h_0 = 400$ m. The results are compared with the observed u and η in *figure 11* where it can be seen that the uniform potential vorticity model leads to a structure which is qualitatively similar to that observed but predicts the width of the stream as 10 km which is about a half of that observed and predicted by the JEBAR model.

6. THE RELATIONSHIP BETWEEN THE SALINITY AND VELOCITY MAXIMA

An interesting and surprising feature of the results is the displacement of the salinity anomaly relative to the current maximum (*figure 12a*) with the high salinity region consistently closer to the slope than the core of the slope current. If, as suggested by Hill and Mitchelson-Jacob (1993), the salinity anomaly arises from the advection of saltier water from the south, we might expect a close correlation of salinity and velocity. That such a close correlation is not observed may result from the different boundary conditions applying to the cross-slope diffusion of salinity and momentum. For a depth uniform flow at speed V parallel to a vertical boundary (*figure 12b*), a steady state balance between advection and cross-stream diffusion may be written:

$$K_x \frac{\partial^2 S}{\partial x^2} = V \frac{\partial S}{\partial y} = -C_s \qquad (10)$$

$$N_x \frac{\partial^2 V}{\partial x^2} = V \frac{\partial V}{\partial y} = -C_v$$

for salt and momentum respectively. The advective driving terms may be supposed uniform in the region of interest with C_s and C_v being positive constants. The corresponding boundary conditions at the vertical wall will be:

$$K_x \frac{\partial S}{\partial x} = 0; \; N_x \frac{\partial V}{\partial x} = \frac{\tau}{\rho} \qquad (11)$$
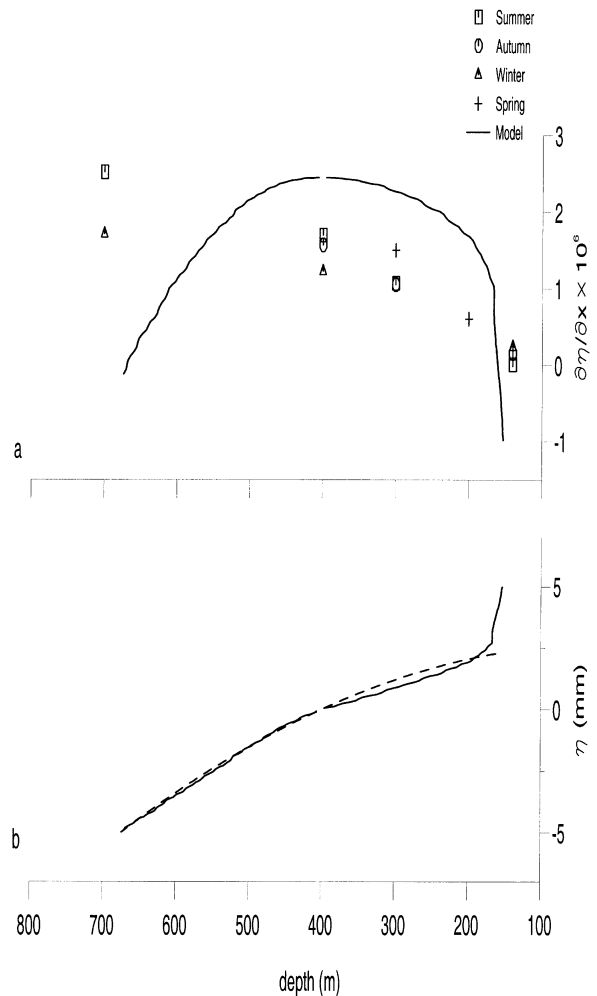

Figure 11. Homogenous vorticity model. (a) $\partial\eta/\partial x$ versus depth, the continuous line represents calculations from realistic topography using homogenous vorticity arguments; points are calculated from observations using the geostrophic assumption, (b) η versus depth, the continuous line is computed from vorticity arguments and dashed line derived from the functional fit of observations.

where τ is the retarding stress at the boundary. The solutions for salinity and velocity are then just:

$$S = S_0 - \frac{C_s x^2}{2K_x} \qquad (12)$$

$$V = V_0 + \frac{\tau}{N_x \rho} x - \frac{C_v}{2N_x} x^2$$

where S_0 and V_0 are the values of salinity and velocity on the boundary. This simple model implies a maximum

Figure 13. Schematic of the slope current, showing the principal features observed: the steady barotropic slope current and associated Ekman draining generated by the bottom stress of the current.
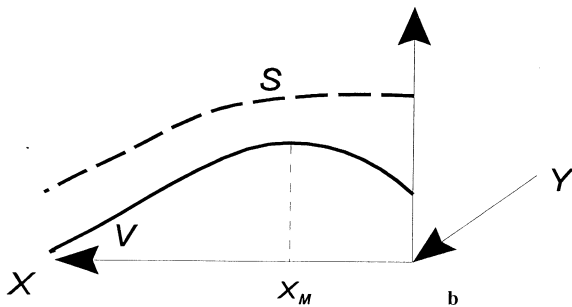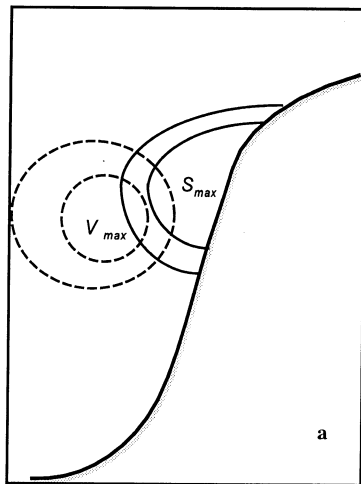
Figure 12. Schematic of slope current and salinity anomaly. (a) Schematic of cross-slope section showing different positions of velocity (*V*) and salinity (*S*) cores as suggested by the data. (b) Schematic of a depth uniform flow at speed *V* parallel to a vertical boundary where there is a steady balance between advection and cross-stream diffusion; note that the salinity has a maximum at $x = 0$ while the velocity maximum is at $x = x_\mathrm{m} = \tau/(\rho\ C_\mathrm{v})$.

salinity at the boundary while the velocity maximum is displaced offshore a distance of $\tau/(\rho\ C_\mathrm{v})$ as indicated in *figure 12b*. Whereas momentum is absorbed at the boundary through the frictional stress, there is no equivalent sink for salinity whose diffusion is effectively reflected at the boundary.

7. DISCUSSION

The picture that emerges from these observations of the slope current (*figure 13*) is of a persistent, predominantly barotropic, flow extending outwards from the top of the slope into water depths > 700 m. Within the core of the
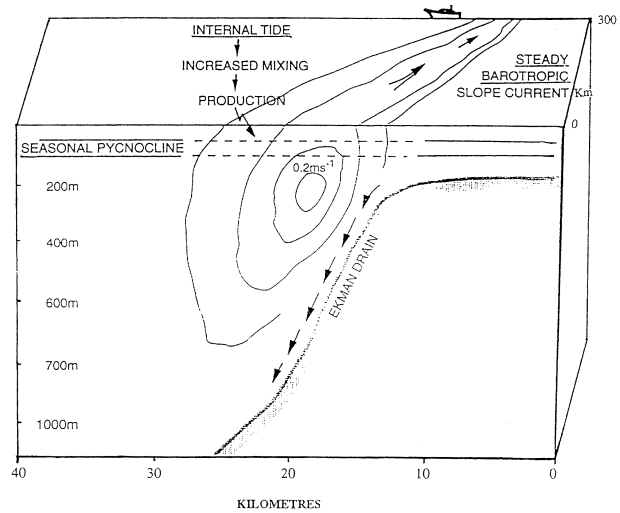
current, the flow is remarkably steady with St up to 0.8 and essentially parallel to the topography. There is a significant baroclinic component to the flow in summer but even then, a large proportion (> 80) of the mean flow kinetic energy resides in the barotropic current. The flow was found to be significantly stronger in the winter months when it is also more variable. In January and February 1996 there was clear evidence of strong northward flows intruding onto the shelf. It seems likely that these changes are associated with an increased windstress forcing during the winter.

As we might expect for a rather steady barotropic geostrophic flow, the current vectors are closely parallel to the isobaths, especially in summer when the cross-slope velocity is generally of order $2\ \mathrm{cm \cdot s^{-1}}$ or less. In the winter period there was an apparently stronger cross-slope flow of up to $4\ \mathrm{cm \cdot s^{-1}}$ offshore which may be associated with strong windstress, predominantly directed to the south during the observational period. Sea surface topography, computed on the basis of the observed currents suggests a consistent relation to the bathymetry. The form of the functional relationship involved is not constrained by theory but is reasonably consistent between different sampling periods over the seasonal cycle. The observed current structure is of the form indicated by a theory based on JEBAR forcing but a plausible description is also given by simple uniform potential vorticity. It would, therefore, be premature to draw any strong conclusions about

JEBAR forcing at this stage but the use of current structure as a diagnostic for forcing may have potential as more comprehensive data sets become available.

An obvious weakness of the observations is that the array did not extend far enough westwards into deep water to define the outer boundary of the flow and determine the full transport of the slope current. The ship-borne ADCP data indicates that strong flow continues to at least the 1 000-m isobath (as suggested by the JEBAR fitting) although the sampling is sparse. The temperature and salinity sections indicate that the flow extends ≈ 20 km from the top of the slope and this is confirmed by further inferences of the width of the stream, which come from drifter tracks. Measurements with the SES drifter clusters Burrows et al. (1999) suggest that the strong, bathymetrically steered flow is confined within the 1 500-m contour which implies a width of ≈ 25 km and barotropic transport ≈ $2 \cdot 10^6$ m³·s⁻¹.

Finally we should note that the frictional stress exerted at the bottom boundary by the slope current is of importance in that it will tend to induce a down-slope component in the slope boundary layer (*figure 13*). Since the slope current is predominantly barotropic, the applied stress will be of order $k \rho V^2$ so that the Ekman transport down the slope is just:

$$Q_E = \frac{\tau}{\rho f} = \frac{kV^2}{f} \qquad (13)$$

where k is the bottom drag coefficient ($2.5 \cdot 10^{-3}$). For V is the along-slope barotropic flow of order of 15 cm·s⁻¹ and the Coriolis parameter $f = 1.2 \cdot 10^{-4}$ s, the cross-slope transport is ≈ 0.46 m²·s⁻¹. Indications of this transport were apparent at S200 and S400 in the summer regime although uncertainties in the determination of cross-slope velocities are of the same order as the observed mean. Nevertheless, in view of the generally weak cross-slope transport, we may infer that this Ekman draining in the boundary layer, which totals $0.3 \cdot 10^6$ m³·s⁻¹ when integrated along the 600 km length of the Hebridean shelf is likely to be an important contributor to cross-shelf exchange.

REFERENCES

Burrows, M., Thorpe, S.A., Meldrum, D.T., 1999. Dispersion over the Hebridean and Shetland shelves and slopes. Cont. Shelf Res. 19, 49–55.

Godin, G., 1972. The Analysis of Tides. Liverpool University Press, Liverpool.

Hill, A.E., Mitchelson-Jacob, E.G., 1993. Observations of a poleward-flowing saline core on the continental slope west of Scotland. Cont. Shelf Res. 40, 1521–1527.

Huthnance, J.M., 1984. Slope currents and 'JEBAR'. J. Phys. Oceanogr. 14, 795–810.

Huthnance, J.M., 1986. The Rockall slope current and shelf-edge processes. In: Mauchline, J. (Ed.), The oceanography of the Rockall Channel. Proc. Roy. Soc. 88B, Edinburgh, pp. 83–101.

McCartney, B.S., Huthnance, J.M., 1995. RRS Charles Darwin Cruise CD91, 2 March–2 April1995 LOIS Shelf Edge Study. Proudman Oceanogr. Lab. Cruise Rep. 20..

Neumann, G., 1968. Ocean Currents, Oceanography Series 4. Elsevier, Amsterdam.

Pingree, R.D., Griffiths, D.K., Mardell, G.T., 1983. The structure of the internal tide at the Celtic Sea shelf break. J. Mar. Biol. Assoc. UK 64, 99–113.

Pingree, R.D., Le Cann, B., 1989. Celtic and Armorican slope and shelf residual currents. Progr. Oceanogr. 23, 303–338.

Proudman, J., 1953. Dynamical Oceanography. Methuen and Co., London.

Sarkisyan, A.S., Ivanov, V.F., 1971. The combined effect of baroclinicity and bottom relief as an important factor in the dynamics of ocean currents. Izv. Acad. Sci. USSR, Atmos. Oceanic Phys. (AGU translation), pp. 173–188..

Simpson, J.H., Mitchelson-Jacob, E.G., Hill, A.E., 1990. Flow structure in a channel from acoustic Doppler current profiler. Cont. Shelf Res. 10, 589–603.